Science Advances
AAAS

advances.sciencemag.org/cgi/content/full/5/7/eaaw5798/DC1

Supplementary Materials for

Universal quantized thermal conductance in graphene

Saurabh Kumar Srivastav, Manas Ranjan Sahu, K. Watanabe, T. Taniguchi, Sumilan Banerjee, Anindya Das*

*Corresponding author. Email: anindya@iisc.ac.in

Published 12 July 2019, *Sci. Adv.* **5**, eaaw5798 (2019)
DOI: 10.1126/sciadv.aaw5798

This PDF file includes:

Section S1. Device characterization and measurement setup
Section S2. Gain of the amplification chain
Section S3. Electron temperature (T_0) determination
Section S4. Partition of current and contact resistance
Section S5. Dissipated power in the floating reservoir
Section S6. Determination of the temperature (T_M) of floating reservoir
Section S7. Extended excess thermal noise data
Section S8. Heat loss by electron-phonon cooling
Section S9. Accuracy of the thermal conductance measurement
Section S10. Discussion on heat Coulomb blockade
Fig. S1. Optical image and device response at zero magnetic field.
Fig. S2. Experimental setup for noise measurement.
Fig. S3. Schematic used to derive the gain in section S2.
Fig. S4. Gain of amplification chain: Output voltage from a known input signal in QH state at resonance frequency.
Fig. S5. Gain of amplification chain: From the temperature-dependent thermal noise.
Fig. S6. Gain of amplification chain during measurement of device 3 (graphite back-gated device).
Fig. S7. RC filter assembly and thermal anchoring on the cold finger.
Fig. S8. Electron temperature (T_0) determination.
Fig. S9. Electron temperature (T_0) determination: From shot noise measurement in a p-n junction of graphene device.
Fig. S10. Equipartition of current in left and right moving chiral states.
Fig. S11. Determination of contact resistance and source noise.
Fig. S12. Extended excess thermal noise raw data.
Fig. S13. Extended data of device 1 at B = 6 T.
Fig. S14. Extended data of device 2 at B = 6 T.
Fig. S15. Extended data of device 3 (graphite back gate) at B = 7 T.
Fig. S16. Extended data of device 3 (graphite back gate) at B = 7 T.

Fig. S17. Heat loss by electron-phonon coupling.
Table S1. Gain of amplification chain.
Table S2. Electron temperature (T_0).
Table S3. Contact resistance and the source noise.
Table S4. Contact resistance and the source noise of device 3 (graphite back-gated device).
Table S5. Change in thermal conductance for different electron temperature T_0.
References (*43–55*)

Section S1. Device characterization and measurement setup

We have measured the two terminal total resistances (R) of device-1, device-2 and device-3 (graphite back gate) as a function of gate voltage (V_{BG}) at zero magnetic field. The measured data is fitted with the following equation(43)

$$R = R_C + \frac{L}{We\mu\sqrt{(n_0^2 + (\frac{C_{BG}(V_{BG}-V_{CN})}{e})^2)}} \tag{1}$$

where R_C, L, W, μ, and e are the contact resistance, length, width, mobility, and electron charge, respectively. Carrier concentration of channel is $\frac{C_{BG}(V_{BG}-V_{CN})}{e}$ with C_{BG} and V_{CN} are the capacitance per unit area of back gate and voltage at the charge neutrality point, respectively. n_0 is the charge inhomogeneity.

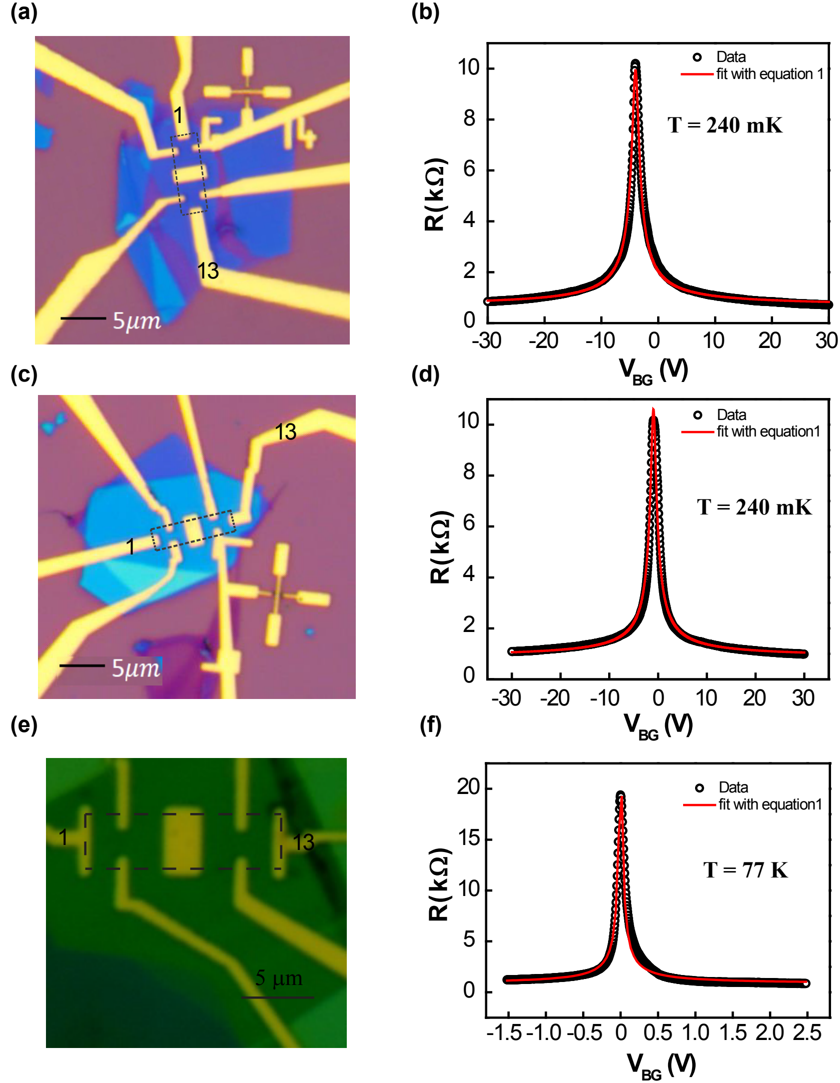

Fig. S1. Optical image and device response at zero magnetic field. The one dimensional edge contacted devices were fabricated using standard dry transfer technique as discussed in materials and methods section in manuscript. (**a,c**) Apart from the conventional quantum Hall (QH) geometry, there is a floating metallic reservoir of area $\sim 6\mu m^2$ and $\sim 4\mu m^2$ of device-1 and device-2, respectively. (**b,d**) Two probe gate response (measured along two extreme ends marked as 1 and 13 in fig (a,c)) at 240 mK using standard Lock-in technique. Open circle shows the data and the red curve is the fit of data in accordance to equation 1 of section S1. This fit gives the mobility $\sim 100000\ cm^2V^{-1}s^{-1}$ and $\sim 110000\ cm^2V^{-1}s^{-1}$ of device-1 and device-2, respectively. (**e**) The optical image of the graphite back gated device with floating reservoir area of $\sim 7\mu m^2$. (**f**) Gate response of the device-3 (graphite back gate) with mobility $\sim 100000\ cm^2V^{-1}s^{-1}$ at 77 K for hole side.

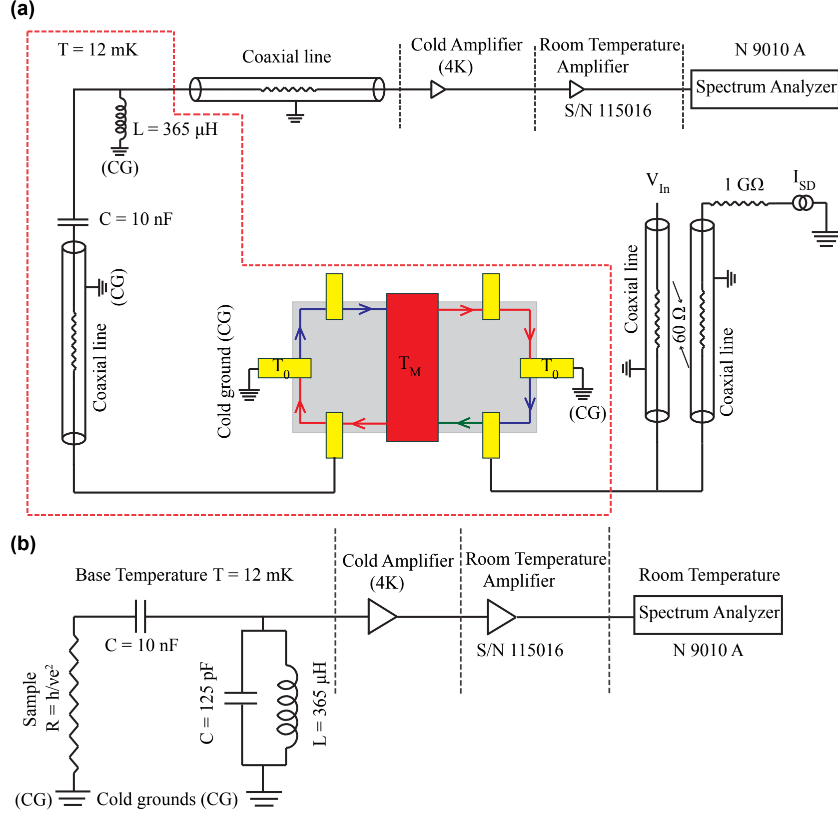

Fig. S2. Experimental setup for noise measurement. (**a**) Schematic of measurement set-up. The device was fixed to the mixing chamber plate of dilution refrigerator in Hall probe configuration with cold grounds. The sample was current biased with a 1 GΩ resistor located at the top of fridge to avoid the extra unwanted noise. Current fluctuations are converted on chip into voltage fluctuations using the well defined quantum Hall (QH) resistance $R = h/\nu e^2$ (as shown schematically in fig(**b**)) where ν is the filling factor. The signal was amplified with a home made cryogenic voltage pre-amplifier, which is thermalized to 4K plate of dilution refrigerator. This pre-amplified signal was then amplified using a voltage amplifier (PR-E3-SMA S/N 115016) placed at room temperature. After second stage of amplification, signal was measured by a spectrum analyzer (N9010A). We have used the band width of $\sim$ 30 kHz. Inductor L $\sim$ 365 μH of the L//C tank was made of an superconducting coil thermally anchored to the mixing chamber of dilution refrigerator. The parallel C $\sim$ 125 pF is the capacitance that develops along the coaxial lines connecting the sample to the cryogenic pre-amplifier. A ceramic capacitance of 10 nF was used between sample and inductor to block the DC current along the measurement line. The typical input voltage noise and current noise of cryogenic pre-amplifiers were $\sim$ 0.25-0.3 $nV/\sqrt{Hz}$ and $\sim$ 10-20 $fA/\sqrt{Hz}$, respectively. (**b**) The schematic circuit diagram of the measurement setup.

Section S2. Gain of the amplification chain

We have used two different methods to calculate the overall gain (G) of amplification chain. (i) Measurement of output voltage for a known input signal in quantum Hall states at resonance frequency; (ii) From temperature dependent Johnson-Nyquist noise (thermal noise)(44).

Output voltage in quantum Hall states: In quantum Hall (QH) regime, one can directly find the relation between source voltage and the output voltage for our device geometry. In our device geometry, the voltage probe which is the part of amplification chain will always see the equilibrium potential of floating reservoir in integr quantum Hall regime. Using Landauer-Buttiker formalism, we have derived the relation between potential of floating reservoir and source contact. In experiment, we have measured the voltage V_{in} at the source contact using a seperate coaxial line as shown in fig. S2. The output voltage V_{out} is measured along the amplification chain using spectrum analyzer. To derive the relation between the output voltage V_{out} and the V_{in}, a schematic figure (fig. S3) is used, in which contacts '1' and '2' represent the two cold grounds. Floating contact and the source contact are shown by contacts '3' and '4', respectively. According to this nomenclature $V_{in} = V_4$. Using Landauer-Buttiker formalism(45), we get

$$\begin{pmatrix} I_1 \\ I_2 \\ I_3 \\ I_4 \end{pmatrix} = \begin{pmatrix} 0 & 0 & \nu G_0 & 0 \\ 0 & 0 & \nu G_0 & 0 \\ \nu G_0 & 0 & 0 & \nu G_0 \\ 0 & \nu G_0 & 0 & 0 \end{pmatrix} \begin{pmatrix} V_1 \\ V_2 \\ V_3 \\ V_4 \end{pmatrix}$$

Here G_0 is the quantum of conductance ($G_0 = e^2/h$). From above matrix we will find following relation

$$I_1 = \nu G_0 V_3 \tag{2}$$

$$I_2 = \nu G_0 V_3 \tag{3}$$

$$I_3 = \nu G_0 V_1 + \nu G_0 V_4 \tag{4}$$

$$I_4 = \nu G_0 V_2 \tag{5}$$

As we have used two cold grounds in our measurement setup, so in fig. S3, 1 and 2 electrodes are grounded i.e. $V_1 = V_2 = 0$ we find

$$I_3 = \nu G_0 V_4 \tag{6}$$

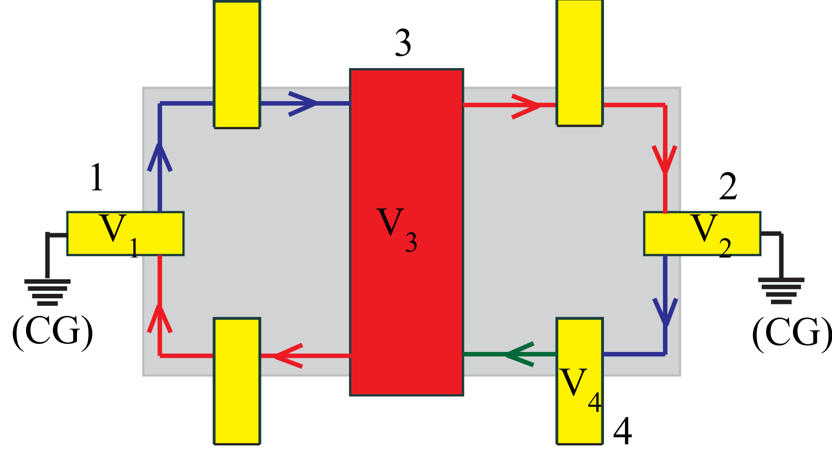

Fig. S3. Schematic used to derive the Gain in section S2.

so

$$V_4 = I_3/\nu G_0 \tag{7}$$

but I_3 is nothing but it is the impinging current in floating reservoir. In equilibrium

$$I_3 = I_1 + I_2 \tag{8}$$

using equation (2), (3), (4), and (6), we obtain

$$V_3 = V_4/2 \tag{9}$$

Electrode which is connected to the amplification circuit will see the voltage V_3. Spectrum analyzer output will give us the voltage V_{out} which is given by

$$V_{out} = GV_3 \tag{10}$$

where G is the gain of amplification chain. Now gain will be given by

$$G = V_{out}/V_3 = 2(V_{out}/V_4) = 2(V_{out}/V_{in}) \tag{11}$$

Temperature dependent thermal noise: In absence of any source current, equilibrium voltage noise spectrum

$$S_V = G^2(4k_BTR + V_n^2 + i_n^2R^2)BW \tag{12}$$

with k_B the Boltzmann factor and T the temperature, V_n^2 and i_n^2 are the intrinsic voltage and current noise density of the amplifier, and BW is the frequency bandwidth. For a fixed integer quantum Hall plateau, change in temperature of mixing chamber (MC) plate will only affect the first term in equation (12), other terms are independent of temperature. So for two different MC plate temperature.
for temperature T_1

$$S_V(T_1) = G^2(4k_BT_1R + V_n^2 + i_n^2R^2)BW \tag{13}$$

and for temperature T_2

$$S_V(T_2) = G^2(4k_BT_2R + V_n^2 + i_n^2R^2)BW \tag{14}$$

subtracting equation (13) from (14), we get

$$G = \sqrt{\frac{S_V(T_2) - S_V(T_1)}{4k_B(T_2 - T_1)BW}} \tag{15}$$

If one plots the $\frac{S_V}{BW}$ as a function of temperature T, slopes of the linear fit will give $4G^2k_BR$, which directly gives the gain of amplification chain and from intercept, intrinsic noise of amplifier can be found.

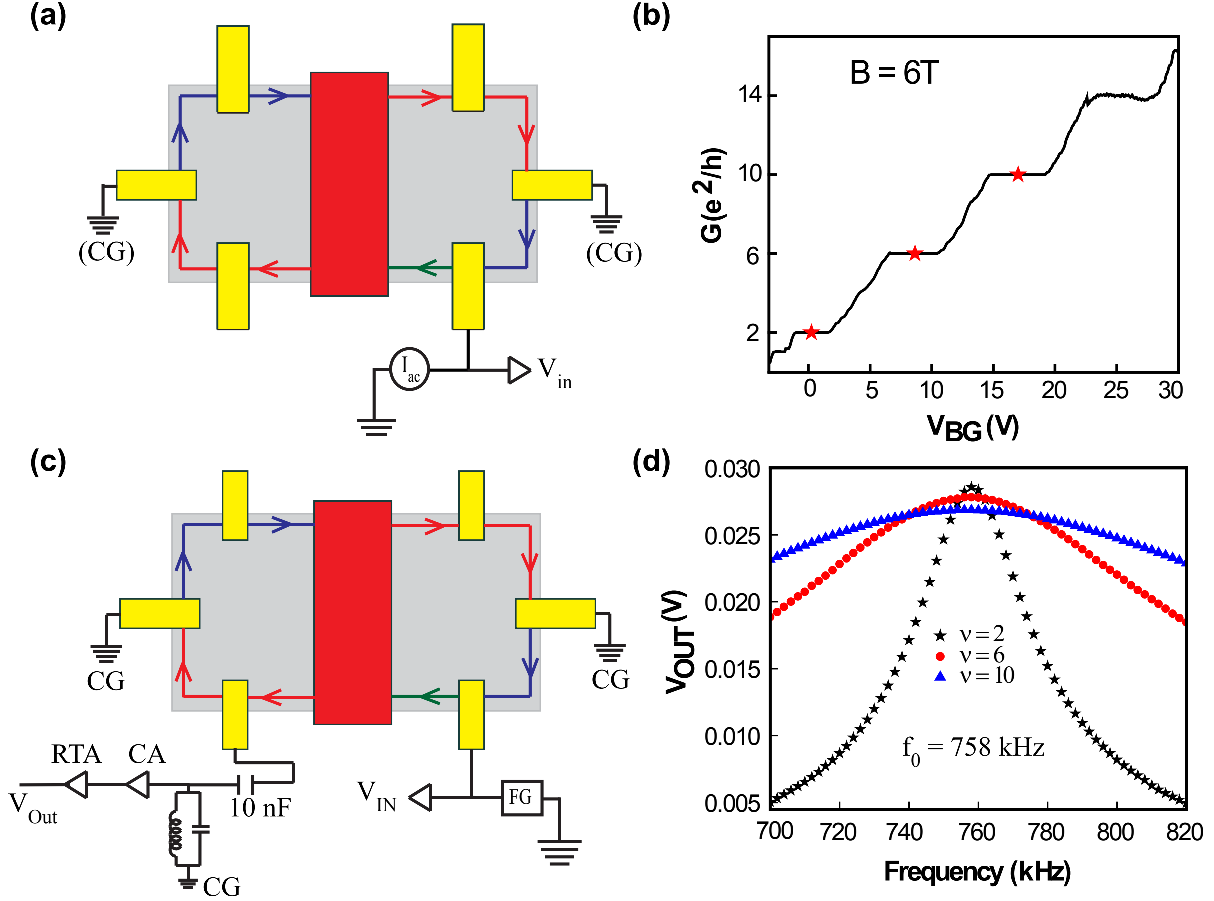

Fig. S4. Gain of amplification chain. (**Output voltage from a known input signal in QH state at resonance frequency:**) (**a**) Schematic of the measurement used to measure conductance using Lock-in amplifier (228 Hz). (**b**) Gate response of Device-1 at B = 6T using low frequency Lock-in technique. Clear plateau in conductance at 2, 6 and 10 are observed in unit of e^2/h. Red stars display the gate voltages at which we have measured the output voltage for given input signal at high frequency. (**c**) Schematic of the measurement used to measure the output voltage for given input voltage in quantum Hall regime at high frequency (758 kHz). A high frequency signal is applied with function generator and voltage V_{in} is measured using the co-axial line as shown in fig. S2). CA and RTA stand for "cold amplifier" and "room temperature amplifier", respectively. (**d**) Output voltage V_{Out} is measured using spectrum analyzer and is plotted as a function of frequency for filling factors of $\nu = 2$, 6 and 10. From the output voltage at resonance frequency, gain is calculated using $G = 2(\frac{V_{Out}}{V_{in}})$ (see section S2). Calculated value of gain is shown in table S1.

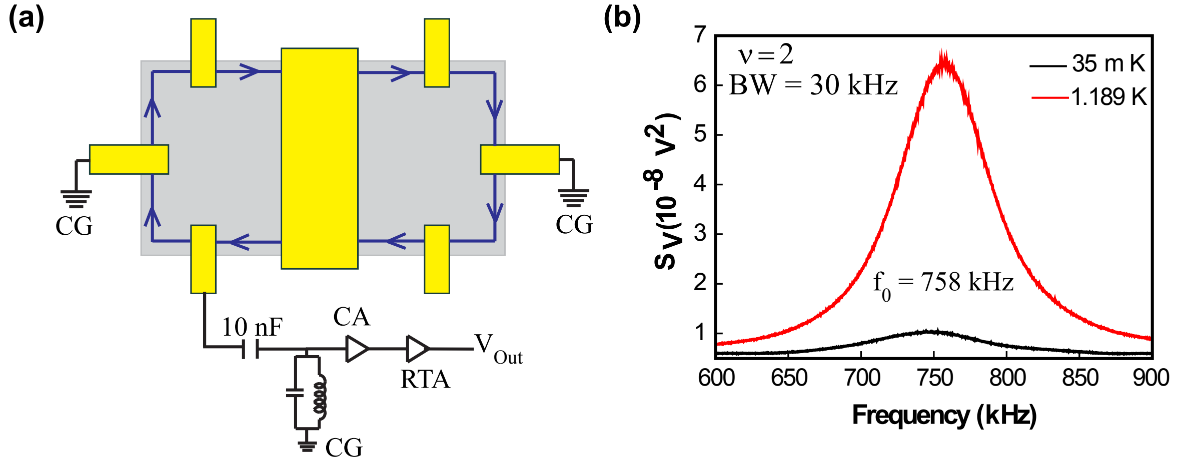

Fig. S5. Gain of amplification chain. (**From temperature-dependent thermal noise**) (**a**) Schematic of the measurement used to measure thermal noise. CA and RTA stand for "cold amplifier" and "room temperature amplifier", respectively. (**b**) The total noise measured by a spectrum analyzer for device-1 is plotted as a function of frequency at zero bias at temperature $\sim$ 35 mK (black) and 1.189 K (red) (RuO_2 sensor reading) for filling $\nu = 2$. The resonance frequency is observed at $\sim$ 758 kHz clearly visible in the plot. From peak value of these data, gain is calculated using $G = \sqrt{\frac{S_V(T_2)-S_V(T_1)}{4k_B(T_2-T_1)BW}}$ (see section S2). Calculated gain was found $\sim$ 1425, which is closely same as obtained from measurement of output voltage for a known input signal in quantum Hall states at resonance frequency.

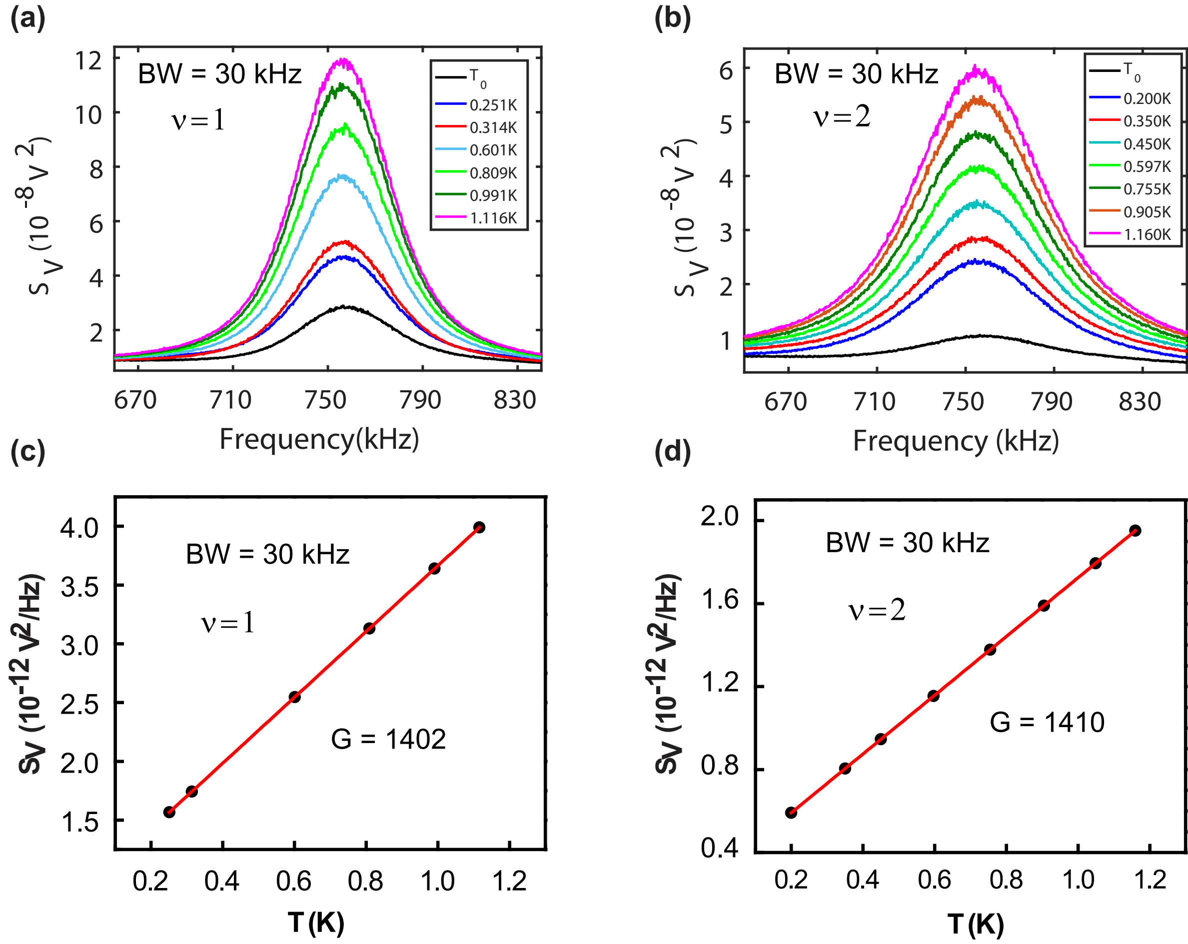

Fig. S6. Gain of amplification chain during measurement of device 3 (graphite back-gated device) (**a**) Noise measured by spectrum analyzer is plotted as a function of frequency at different temperature at $\nu = 1$ and similarly for (**b**) $\nu = 2$. (**c**) Symbols represent the plot of noise divided by bandwidth (BW) at resonance frequency as a function of temperature at $\nu = 1$. Solid red line is the linear fit of data and from the slope of this line, calculated gain was found to be equal to ∼1402. (**d**) Symbols represent the plot of noise divided by bandwidth (BW) at resonance frequency as a function of temperature at $\nu = 2$. Solid red line is the linear fit of data and from the slope of this line, calculated gain was found to be equal to ∼1410. From the intercept of these linear fit of $\nu = 1$ and 2, the V_n and i_n of amplifier were found to be $\sim 246\frac{pV}{\sqrt{Hz}}$ and $\sim 24\frac{fA}{\sqrt{Hz}}$, respectively. Thus, it can be seen that the error in gain is less than 1%.

Table S1. Gain of amplification chain.

Filling Factor(ν)	V_{IN} (μV)	V_{OUT}(mV)	Gain (G) = 2 (V_{OUT} / V_{IN})	Gain from Jhonson Nyquist Noise
2	39.97	28.56	1429.1	
6	39.03	27.80	1424.5	1425
10	37.54	26.84	1429.9	

Section S3. Electron temperature (T_0) determination

Electron temperature for device-1 and device-2: In this section we will discuss how we have extracted out the electron temperature of the devices. For device-1 and device-2 we have used coaxial line as input as shown in fig. S2, where the $\sim$ 60 ohm resistance and $\sim$1 nF capacitance of the line work as low-pass filter. In this setup we have measured the thermal noise at different filling and from which we have extracted the electron temperature as shown in fig. S8 and table S2. To cross check we have measured the shot noise at a graphene pn junction using same coaxial lines and extract out the electron temperature as shown in fig. S9. The average electron temperature using coaxial line in our experiment was $T_0 \sim 40$ mK.

Electron temperature for device-3(graphite back gate): For device-3 (graphite back gated device) we have introduced extra low-pass filter made of 200 ohm and 1 nF capacitor in input line at the mixing chamber to lower the electron temperature which can be seen from the photograph of cold finger in fig. S7. As we have mentioned earlier in section S2, that noise measured by spectrum analyzer at zero bias is given by

$$S_V = G^2(4k_BTR + V_n^2 + i_n^2R^2)BW \tag{16}$$

If one plots the $\frac{S_V}{BW}$ as a function of temperature at fixed quantum Hall filling as plotted in fig. S6(c) and S6(d), the linear fit of the data will give an linear equation which relates the $\frac{S_V}{BW}$ to temperature T directly. Since the gain (from the slope) and intrinsic noise of amplification chain (from the intercept) is already known (see caption of fig. S6), so now from the known value of measured noise at zero bias and base temperature, the corresponding electron temperature can be found directly using the following equation

$$T_0 = \frac{\left(\left(\frac{S_V}{G^2BW}\right) - (V_n^2 + i_n^2R^2)\right)}{4k_BR} \tag{17}$$

As our measured value of noise at base temperature were $2.8180 \times 10^{-8}V^2$ at $\nu = 1$ which corresponds to $T_0 \sim 27$ mK. Similarily, at $\nu = 2$ measured noise was $1.0404 \times 10^{-8}V^2$, which also corresponds to $T_0 \sim 27$ mK.

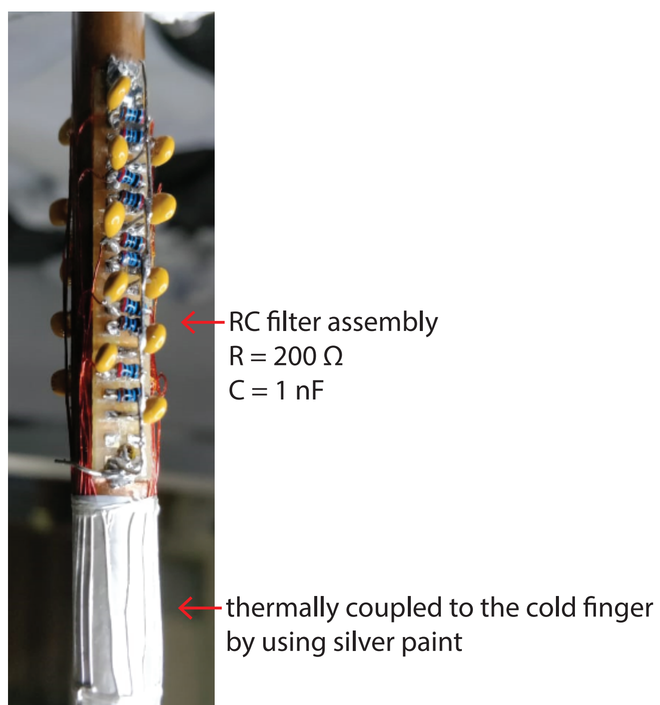

Fig. S7. RC filter assembly and thermal anchoring on the cold finger. (Photo credit: Saurabh Kumar Srivastav, Indian Institute of Science)

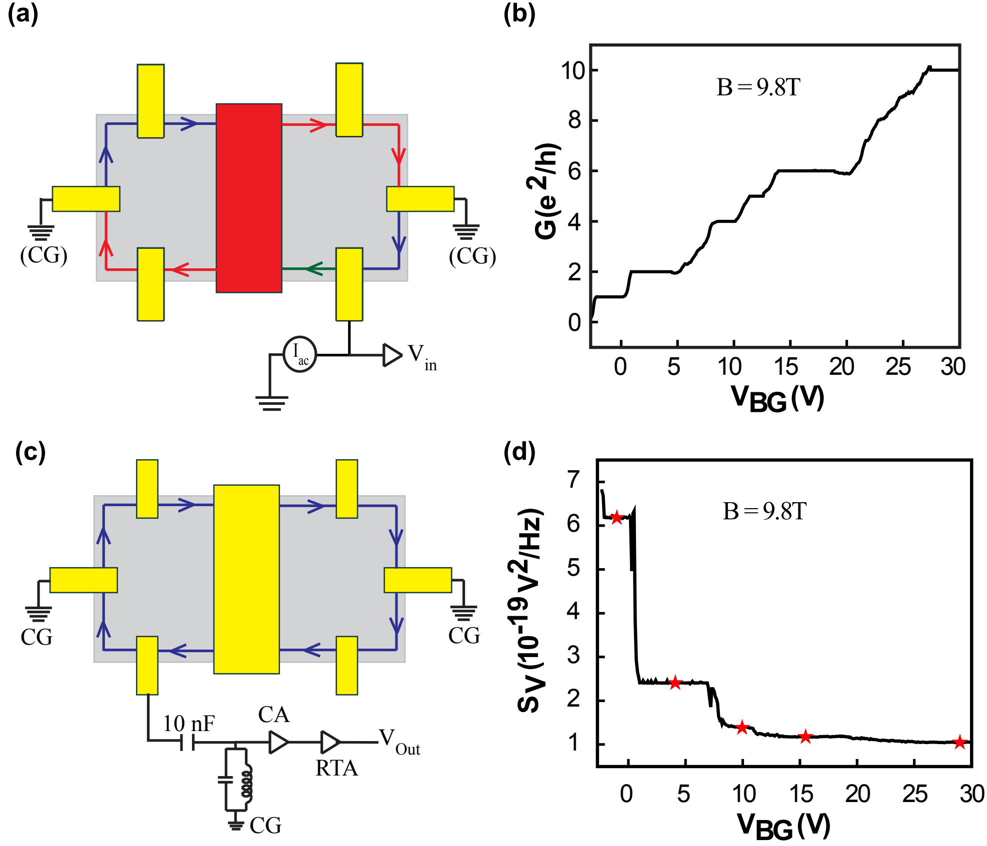

Fig. S8. Electron temperature (T_0) determination. We have used two different methods to find the electron temperature T_0. (i) Measuring the thermal noise for different integer quantum Hall filling. (ii) Measuring the shot noise in p-n junction graphene device in integer quantum Hall regime.

(**From measuring the thermal noise for different integer quantum Hall filling:**) (**a**) Schematic of the measurement used to measure the conductance at low frequency (Lock-in at 228 Hz). (**b**) Gate response of Device-1 at B = 9.8T using low frequency Lock-in technique. Clear plateaus in conductance at 1, 2, 4, 5, 6, and 10 and less developed plateau at 3, 7, 8, and 9 are observed in unit of e^2/h. (**c**) Schematic of the measurement used to measure thermal noise. CA and RTA stand for "cold amplifier" and "room temperature amplifier", respectively. (**d**) The total noise measured by spectrum analyzer is plotted as a function of gate voltages at zero bias at base temperature of mixing chamber plate. Clear plateaus in these data are exactly at the same place as in conductance data. Red stars are the point, whose value we have taken to determine the electron temperature T_0. As mentioned in section S2, total noise measured by spectrum analyzer is $S_V = G^2(4k_BTR + V_n^2 + i_n^2R^2)BW$. Varying the filling factor will only change the R in this equation. So by measuring the total noise S_V at three different fillings, we will get three linearly independent equation in three variables T, V_n, and i_n, which can be solved algebraically. Calculated values are shown in table S2.

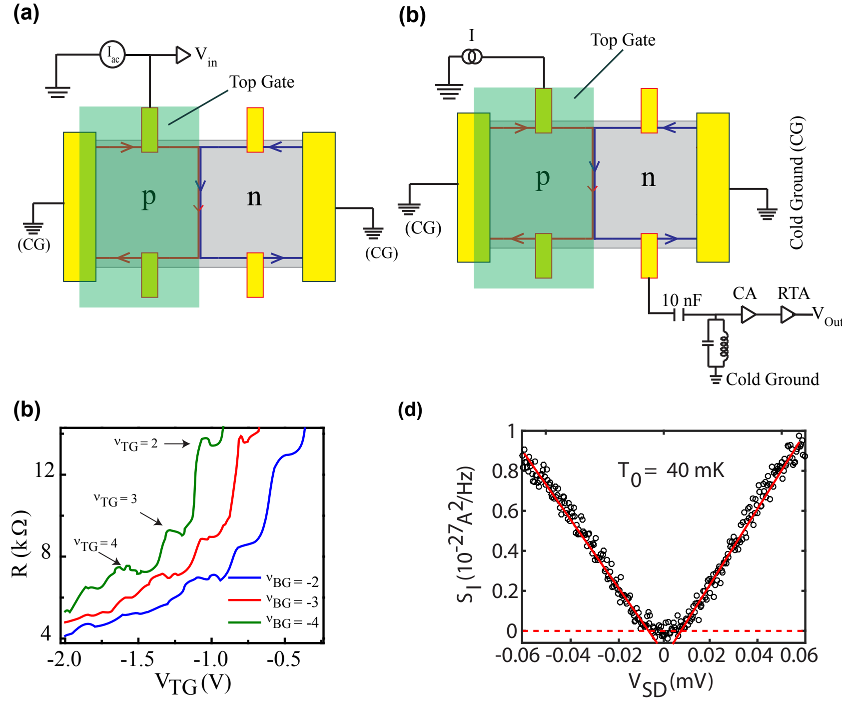

Fig. S9. Electron temperature (T_0) determination. (**From shot noise measurement in a p-n junction of graphene device**) We have done the shot noise measurement in seperate p-n junction graphene device in integer quantum Hall regime using same measurement set-up which we have used for our device-1 and device-2. (**a**) Schematic of the measurement used to measure low frequency (228 Hz) conductance. (**b**) Schematic of the measurement used to measure the shot noise. CA and RTA stand for "cold amplifier" and "room temperature amplifier", respectively. Shot noise is measured using the spectrum analyzer. (**c**) Resistance $\left(\frac{V_{in}}{I_{ac}}\right)$ is plotted as a function of top gate voltage for the fixed filling of back gate of ν = -2 (blue), -3 (red), and -4 (green). For the given filling of back gate, we can see the plateaus as the top gate is scanned. At the plateau $\nu = (4, -4)$, we have measured the shot noise. (**d**) Symbols display the shot noise as a function of V_{SD}, where V_{SD} is related to the applied DC current I as $I = G_{PNJ}V_{SD}$ with G_{PNJ} as electrical conductance across p-n junction(46, 47). The horizonatl dashed line represents the zero noise line. Continuous red lines are the linear fit of these data at higher voltages whose linear extrapolation to zero noise gives $eV_{SD} = 2k_BT_0$ (11). In our case, the linear extrapolation to zero noise gives $V_{SD} \sim 6.95\mu V$. This corresponds to electron temperature $T_0 \sim 40$ mK, which is independent of gain of amplification chain.

Table S2. Electron temperature (T_0). The average temperature T_0 calculated from above table is the (43.8 ± 1.4) mK. This corresponds to 3.2% error in the T_0.

configuration of ν			T_0 (mK)	V_n (nV/√Hz)	I_n (fA/√Hz)
1	2	4	44.7	0.3060	26.29
1	2	6	44.0	0.3066	26.31
1	2	10	44.3	0.3063	26.30
1	4	6	42.1	0.3072	26.37
1	4	10	43.7	0.3064	26.32
2	4	6	41.0	0.3075	26.50
2	4	10	43.4	0.3065	26.36
1	6	10	45.4	0.3061	26.26
2	6	10	45.9	0.3060	26.19

Section S4. Partition of current and contact resistance

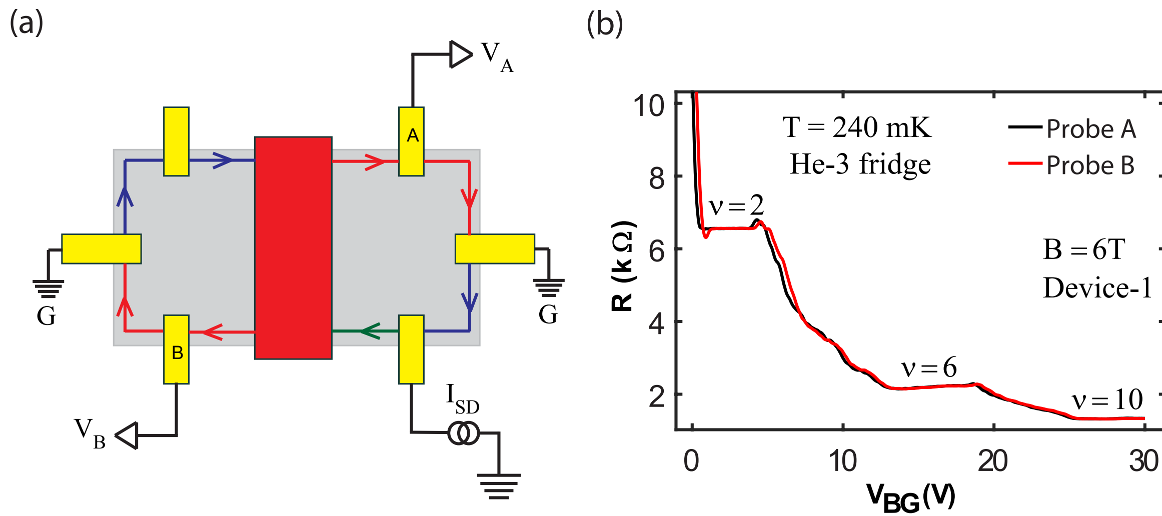

Fig. S10. Equipartition of current in left and right moving chiral states . For a given back gate voltage, filling in both arm of the device should be same. To confirm this we have measured the voltages in both arm of the device-1. (**a**) Current is applied through the source contact and the voltages are measured using probe 'A' and 'B', respectively. (**b**) Voltages divided by the applied current is plotted as a function of gate voltages measured at two different probes 'A' (black) and 'B' (red). It is clearly visible that the voltages measured at two probes are the same.

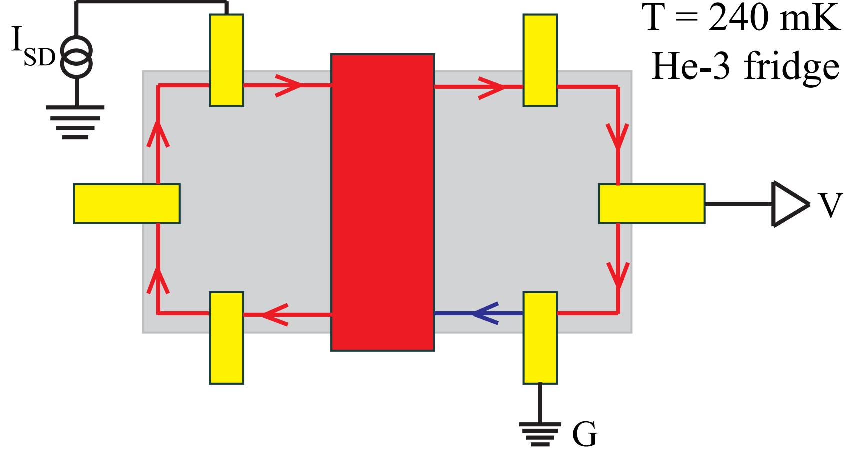

Fig. S11. Determination of contact resistance and source noise. At finite DC bias, if the contacts are not transparent for the edge channels, it will give extra noise, known as source noise whose magnitude will be given as $2eI(1-t)$, where t is the transmittance of source contact. To determine the contact resistance of source contact, we have used the three probe measurement technique. In our device configuration, if voltage probe V is situated in path of hot edge for given chirality, it will measure a voltage $V_H = I.(R_0 + R_L + R_C)$ with R_0-quantum Hall resistance, R_C-contact resistance and R_L-line resistance of ground contact. On the other hand for opposite chirality, it will measure a voltage $V_C = I.R_L$. Differences of these two voltages will give us $I.(R_0 + R_C)$. So conductance is given by $\frac{1}{R_0+R_C}$ hence transmittance t will be given by the ratio of actual resistance and measured resistance, i.e. $t = \frac{R_0}{R_0+R_C}$. Once the transmittance is known, one can easily determine the source noise $2eI(1-t)$. Since amplifier is situated in path of left moving edge channels, it will measure only part of the generated source noise. In particular, for our device configuration, amplifier will always see only the half of total no of edge channels leaving the floating reservoir. Hence it will always measure the only $\frac{1}{4}$th of the source noise. Values of the contact resistance, transmittance and maximum source noise is given in table S3 for device-1 and device-2 and in table S4 for device-3.

Table S3. Contact resistance and the Source noise. Since the reflection was always less than 1% for each filling factor. So the measured source noise could be as maximum as about $0.2 \times 10^{-29} A^2 Hz^{-1}$ at maximum source current which is $\sim$ 80 times smaller than the measured excess thermal noise. Make note that typical line resistance of He-3 fridge was 625-635 Ω, which was measured also seperately.

Device	Filling Factor(ν)	Hot edge $V_H / I = (R_0 + R_L + R_C)$ (Ω)	Cold edge $V_C / I = R_L$ (Ω)	Contact Resistance $(V_H / I - V_C / I) - R_0$ in (Ω)	Trans-mittance (t)	Source Noise / 4 ($10^{-29} A^2 / Hz$) at I_{max}
1	1	26509	635	64	0.9975	0.0495 @ I_{max} = 2.5 nA
	2	13574	635	34	0.9974	0.0736 @ I_{max} = 3.5 nA
	6	4952	635	16	0.9963	0.2075 @ I_{max} = 7.0 nA
2	2	13570	624	41	0.9968	0.1536 @ I_{max} = 6.0 nA
	6	4939	624	13	0.9969	0.2232 @ I_{max} = 6.0 nA

Table S4. Contact resistance and the Source noise of device 3 (graphite back-gate device). Contact resistance of device-3 was measured in dilution refrigerator using low frequency Lock-in technique at 228 Hz. A constant current I was injected at source contact and voltage was measured at the same contact (See the fig. S8(a)). This voltage probe will measure the voltage $I.(R_0 + R_L + R_C)$ with R_0-quantum Hall resistance, R_C-contact resistance and R_L-line resistance. So measured resistance will be $R_0 + R_L + R_C$. We have measured line resistance R_L of 260 Ω seperately. After subtracting the line resistance, conductance will be equal to $\frac{1}{R_0+R_C}$. Hence the transmittance t will be given by $t = \frac{R_0}{R_0+R_C}$. Once the transmittance is known, one can easily determine the source noise (see the caption of fig. S11). So the maximum source noise at maximum current is much lower than the measured excess thermal noise (see fig. S15).

Device	Filling Factor(ν)	Measured resistance ($R_0+R_L+R_C$) (Ω)	Line resistance R_L (Ω)	Contact Resistance ($R_0+R_L+R_C$) - R_L - R_0 in (Ω)	Trans-mittance (t)	Source Noise / 4 ($10^{-29} A^2/Hz$) at I_{max}
3	1	26143	260	73	0.9972	0.0448 @ I_{max} = 2.0 nA
	4/3	19660	260	42	0.9978	0.0264 @ I_{max} = 1.5 nA
	2	13231	260	66	0.9949	0.0816 @ I_{max} = 2.0 nA

Section S5. Dissipated power in the floating reservoir

As mentioned in the manuscript a DC current I, injected at the source contact (Fig. 1a of the manuscript), flows along the chiral edge towards the floating reservoir. The outgoing current from the floating reservoir splits into two equal parts, each propagating along the outgoing chiral edge from the floating reservoir to the cold grounds. The floating reservoir reaches a new equilibrium potential $V_M = \frac{I}{2\nu G_0}$ with the filling factor ν of graphene determined by the V_{BG}, whereas the potential of the source contact is $V_S = \frac{I}{\nu G_0}$. Thus, the power input to the floating reservoir is $P_{in} = \frac{1}{2}(IV_S) = \frac{I^2}{2\nu G_0}$, where the pre-factor of 1/2 results due to the fact that equal power dissipates at the source and the floating reservoirs in Fig. 1a of the manuscript. Similarly, the outgoing power from the floating reservoir is $P_{out} = \frac{1}{2}(2 \times \frac{I}{2}V_M) = \frac{I^2}{4\nu G_0}$. Thus, the resultant injected power dissipation in the floating reservoir due to joule heating is $J_Q = P_{in} - P_{out} = \frac{I^2}{4\nu G_0}$.

Section S6. Determination of the temperature (T_M) of floating reservoir

The resulting increase in the electronic temperature $(T_M - T_0)$ of floating reservoir is determined from the excess thermal noise(7, 11, 48, 49, 50, 51)

$$S_I = 2G^* k_B (T_M - T_0) \tag{18}$$

with

$$\frac{1}{G^*} = \frac{1}{G_L} + \frac{1}{G_R} \tag{19}$$

where G_L and G_R are the conductance of left and right channel respectively. So in our device structure

$$\frac{1}{G^*} = \frac{1}{\nu G_0} + \frac{1}{\nu G_0} \tag{20}$$

hence

$$S_I = \nu k_B (T_M - T_0) G_0 \tag{21}$$

Section S7. Extended excess thermal noise data

In order to measure the excess thermal noise due to very small temperature increment, we have taken the data many times (~ 1000) and we have shown the average data in the manuscript. In the fig. S12(a) and S12(b), we have shown one such raw data and the average one for $\nu = 1$ and 2, respectively.

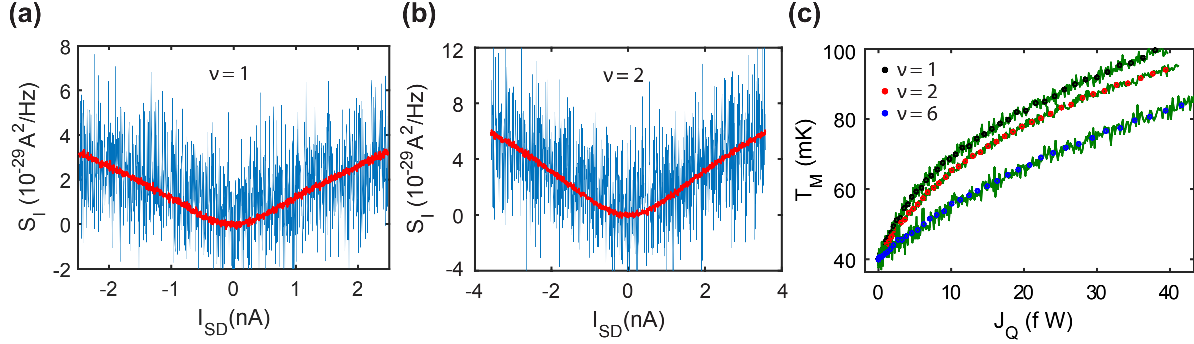

Fig. S12.Extended excess thermal noise raw data. (**a,b**) Excess noise for single scan (blue) and the averaged (red) one for $\nu = 1$ and 2 at B = 9.8T respectively, for device-1. (**c**) Solid curves shows the data extracted directly from raw excess thermal noise data for device-1 at B = 9.8T for $\nu = 1, 2$, and 6 respectively. Solid symbols display the 9 point average of corresponding raw data which is shown in manuscript figure 2(d).

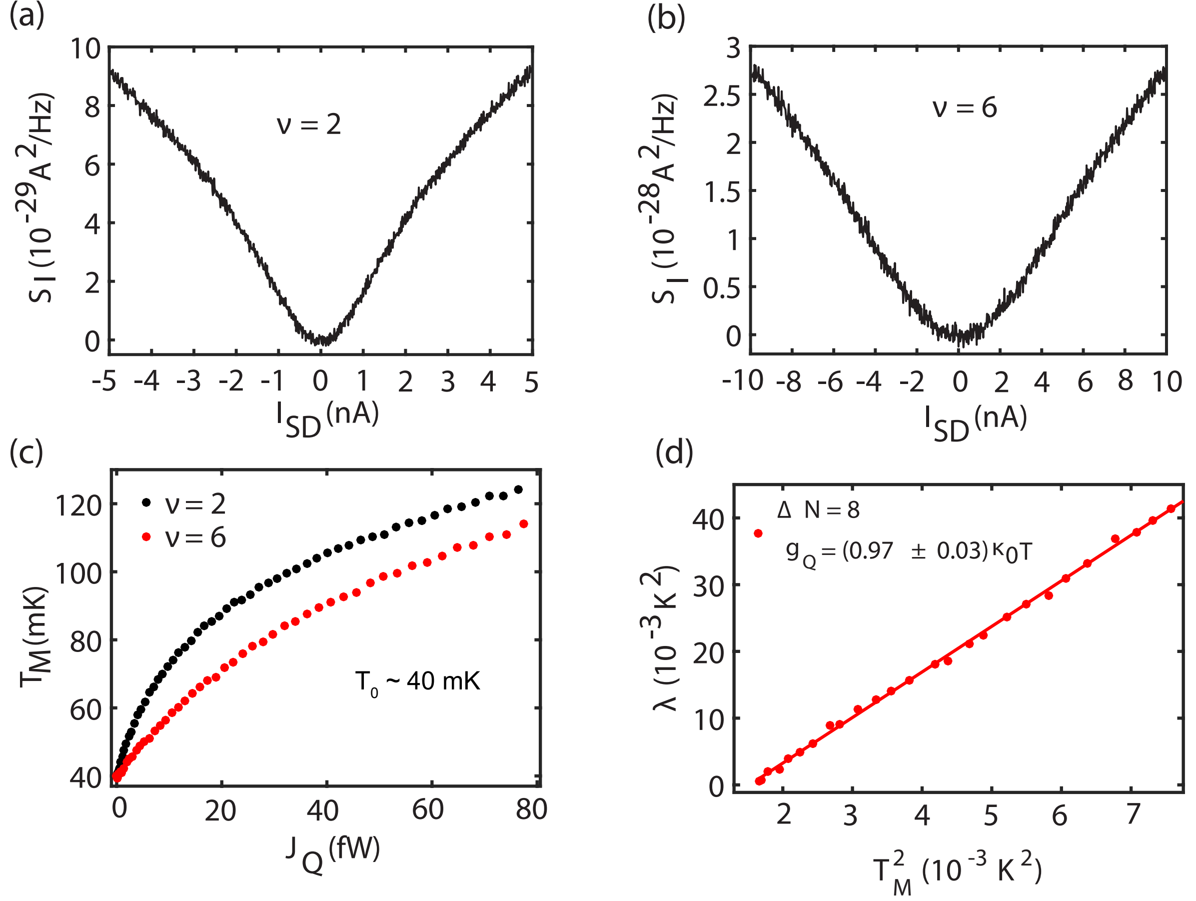

Fig. S13. Extended data of device 1 at B = 6T. (**a**) Excess thermal noise S_I is plotted as a function of source current I_{SD} at filling $\nu = 2$. (**b**) Excess thermal noise S_I is plotted as a function of source current I_{SD} at filling $\nu = 6$. (**c**) Temperature, T_M (it is extracted from the excess thermal noise shown in upper panel) of floating contact is plotted as a function of dissipated power J_Q (obtained using $J_Q = \frac{I^2}{4\nu G_0}$) for two different filling factors $\nu = 2$ and 6, respectively. Symbols display the extracted temperature data using equation $S_I = \nu k_B(T_M - T_0)G_0$. (**d**) The $\lambda = \Delta J_Q/(0.5\kappa_0)$ is plotted as a function of T_M^2 for $\Delta N = 8$ (here $\Delta J_Q = J_Q(\nu_i, T_M) - J_Q(\nu_j, T_M)$). Solid circles display the data and the continuous red curve is the linear fit of these data. Slope of this linear fit is 7.76 which gives $g_Q = 0.97\kappa_0$T with specified error.

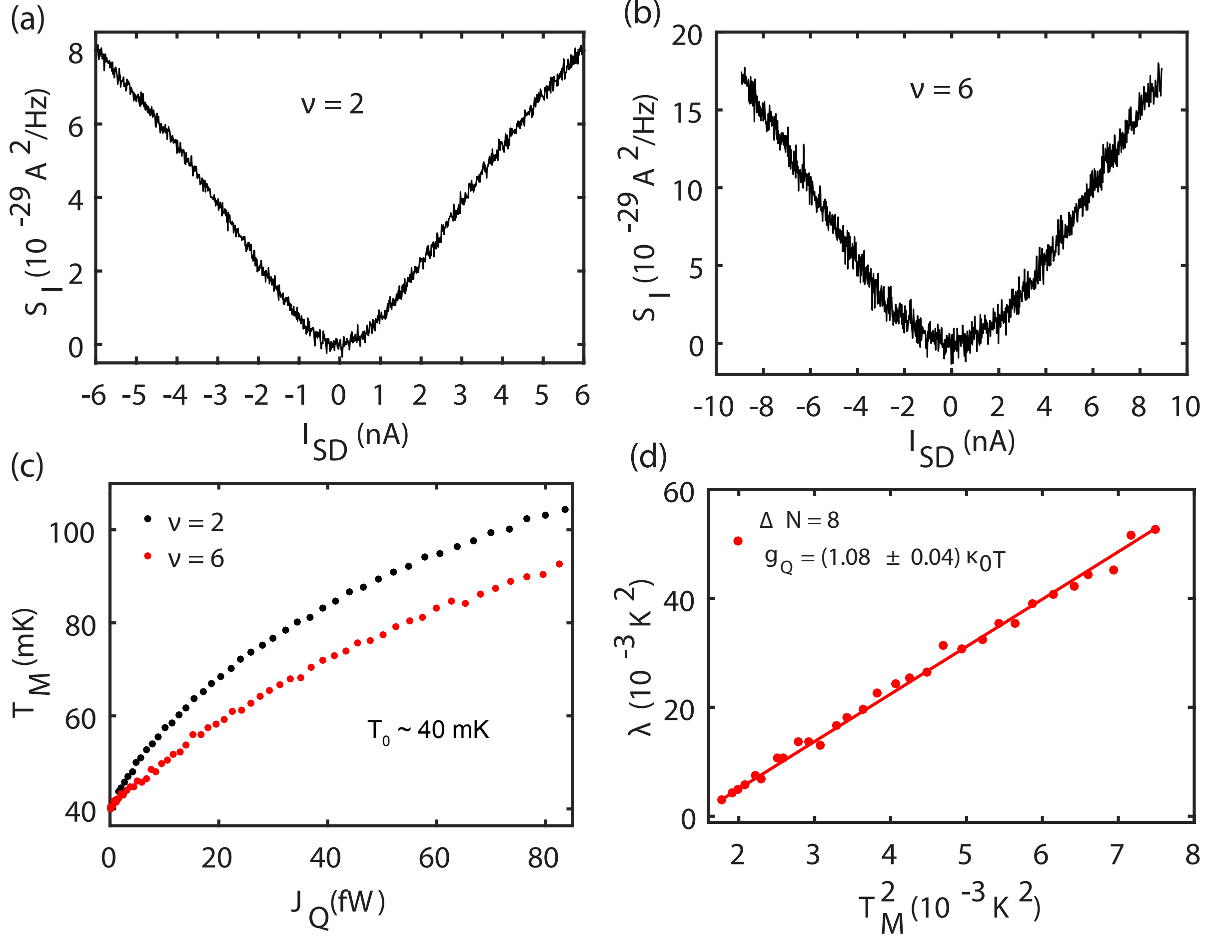

Fig. S14. Extended data of device 2 at B = 6T. (**a**) Excess thermal noise S_I is plotted as a function of source current I_{SD} at filling $\nu = 2$. (**b**) Excess thermal noise S_I is plotted as a function of source current I_{SD} at filling $\nu = 6$. (**c**) Temperature T_M (it is extracted from the excess thermal noise shown in upper pannel) of floating contact is plotted as a function of dissipated power J_Q (obtained using $J_Q = \frac{I^2}{4\nu G_0}$) for two different filling factors $\nu = 2$ and 6, respectively. Symbols display the extracted temperature data using equation $S_I = \nu k_B (T_M - T_0) G_0$. (**d**) The $\lambda = \Delta J_Q/(0.5\kappa_0)$ is plotted as a function of T_M^2 for $\Delta N = 8$ (here $\Delta J_Q = J_Q(\nu_i, T_M) - J_Q(\nu_j, T_M)$). Solid circles display the data and the continuous red curve is the linear fit of these data. Slope of this linear fit is 8.64 which gives $g_Q = 1.08\kappa_0 T$ with specified error.

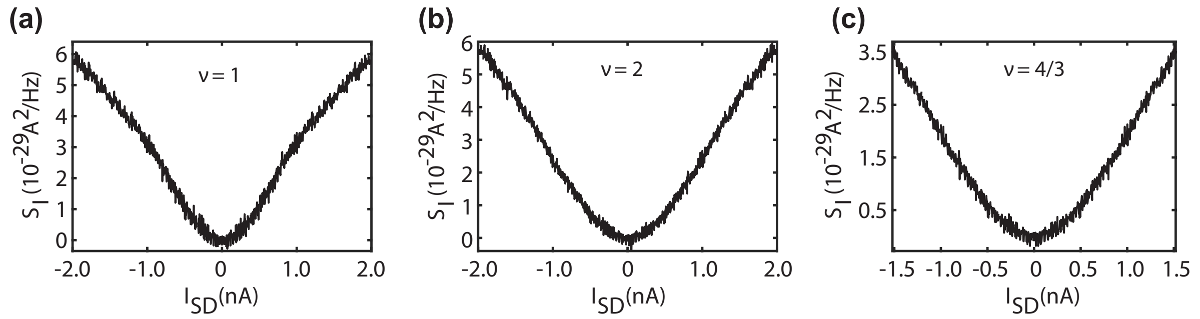

Fig. S15. Extended data of device 3 (graphite back gate) at B = 7T. (a) Excess thermal noise S_I is plotted as a function of source current I_{SD} at filling $\nu = 1$. **(b)** Excess thermal noise S_I is plotted as a function of source current I_{SD} at filling $\nu = 2$ and similarily **(c)** Excess thermal noise S_I is plotted as a function of source current I_{SD} at filling $\nu = 4/3$.

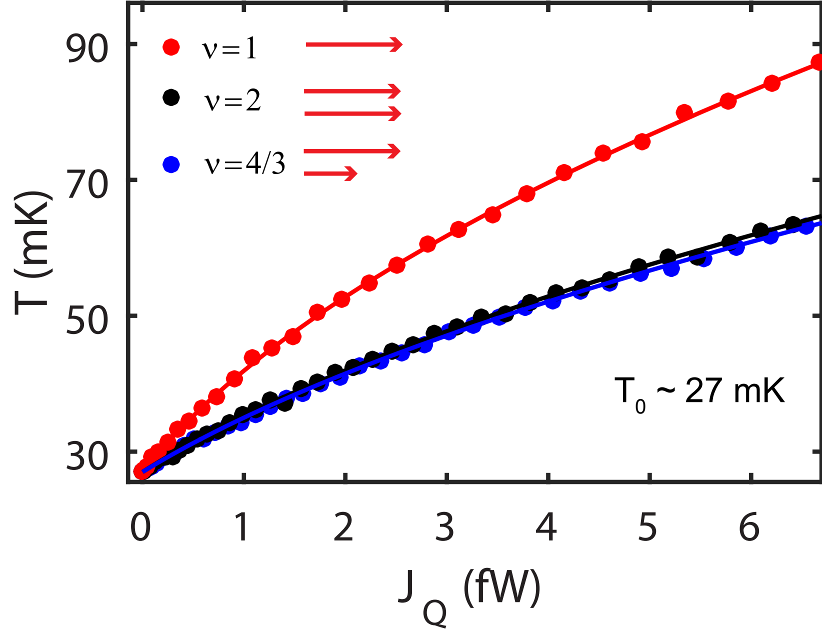

Fig. S16. Extended data of device 3 (graphite back gate) at B = 7T. Temperature T_M (extracted from excess thermal noise plotted in fig. S15) of floating contact is plotted as a function of dissipated power J_Q for filling factors ν = 1, 2, and 4/3. Symbols display the extracted temperature data using equation $S_I = \nu k_B(T_M - T_0)G_0$. Here, the continuous lines are the best fit of data in accordance with equation $J_Q = 0.5N\alpha(T_M^2 - T_0^2)$ (here, we have not included the electron-phonon cooling). There are always two path from floating contact: left moving and right moving channels terminated at respective cold grounds. From fitting α were found to be 1.02, 2.02 and 2.08κ_0 for ν = 1, 2 and 4/3, respectively.

Section S8. Heat loss by Electron-phonon cooling

In this section, we will discuss about the heat transfer via electron-phonon cooling (J_Q^{e-ph}). In steady state, the total dissipated heat power in floating contact (J_Q) is equal to the sum of heat current carried by electronic channels (J_Q^e) and the heat transferred by hot electrons to the cold phonon bath (J_Q^{e-ph}) i.e. $J_Q = J_Q^e + J_Q^{e-ph}$, with $J_Q^e = 0.5N\alpha(T_M^2 - T_0^2)$ and $J_Q^{e-ph} = \beta(T_M^q - T_0^q)$.The temperature exponent of $5-5.8$ has been reported in GaAs 2DEG(39). However, the exponent of 4-6 is predicted depending on the nature of disorders in the floating contact as well as the dimensionality of the phonons involved(52, 53). In our devices, we found the temperature exponent of ~ 4 and ~ 6 for SiO_2 and graphite back gate, respectively as shown in fig. S17. It can be seen from the fig. S17(c) that even up to electron temperature of ~ 90 mK (marked by vertical dashed line), J_Q^{e-ph} is less than 0.1 fW which is quite negligible compared to the electronic contribution in device-3.

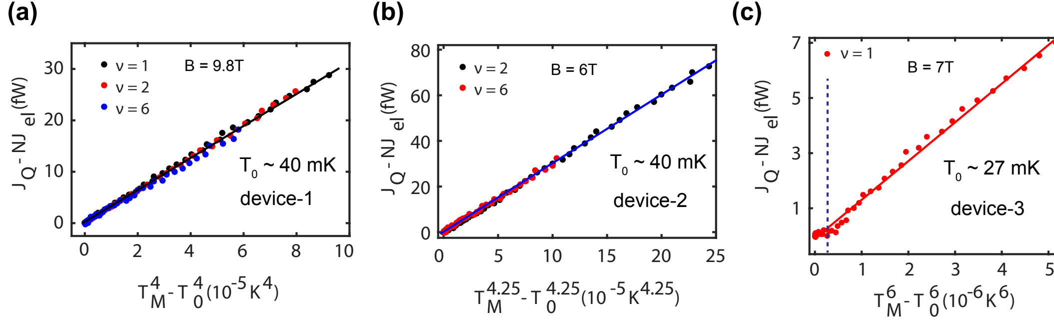

Fig. S17. Heat loss by electron-phonon coupling. (**a**) Solid circles display the electron-phonon contribution of the heat loss, $J_Q^{e-ph} = J_Q - J_Q^e$ with $J_Q^e = NJ_{el} = N0.5\kappa_0(T_M^2 - T_0^2)$ electronic heat flow through N chiral edge channels, as a function of $(T_M^4 - T_0^4)$ for $\nu = 1, 2$, and 6 for device-1. The solid line is the linear fit with a slope, $\beta \sim 0.31nW/K^4$. (**b**) Solid circles display the electron-phonon contribution of the heat loss as a function of $(T_M^{4.25} - T_0^{4.25})$ for $\nu = 1$, and 2 for device-2. The solid line is the linear fit with a slope, $\beta \sim 0.30nW/K^{4.25}$. (**c**) Here, soild circles display the same for device-3 (graphite back gated device) for $\nu = 1$, but it increases with $(T_M^6 - T_0^6)$ with $\beta \sim 1.54nW/K^6$. The vertical dashed line shows that up to $\sim$ 90 mK, J_Q^{e-ph} is very small ($<$ 0.1 fW), which is negligible compared to electronic part. Here, we have not plotted the heat loss to phonon for $\nu = 2$ and 4/3, because at these filling electron-phonon parts were very small. In this device (graphite back gate) the floating reservoir is isolated from the graphite back gate by the bottom hBN but in the case of SiO_2/Si back gated device the floating reservoir is in touch with the SiO_2/Si substrate as the bottom hBN is completely etched out, which might be the reason for different temperature exponent.

Section S9. Accuracy of the thermal conductance measurement

In this section, we will discuss about the accuracy of measured thermal conductance, which requires the careful determination of the parameters of the system. For example: (i) the exact value of total gain of the amplification chain; (ii) the precise measurement of the electron temperature (T_0) and (iii) estimation of generated shot noise due to the finite contact resistance at the graphene QH and electrode junctions. The total voltage gain of

our amplification chain is ∼1402-1425 measured with known input signal as well as measuring the temperature dependent thermal noise in QH plateaus , where the inaccuracy of the gain $\sim 1\%$. The electron temperature, $T_0 \sim 40$mK for device-1 and device-2, was measured in two ways; measuring the thermal noise (together with voltage and current noise of the amplifier) at different filling factors and measuring the shot noise in a graphene pn junction in QH regime. The inaccuracy in our electron temperature measurement is less than 4% as can be seen in table S2. Since the inaccuracy in gain is $\sim 1\%$, so it will not affect measured thermal conductance very much. On the other hand, inaccuracy in electron temperature is $\sim 4\%$, which can be source of major inaccuracy in extracted thermal conductance. So we have calculated the thermal conductance at $T_0 = 40$ mK and 45 mK. The averaged value was found $1.00\kappa_0 T$ at $T_0 = 40$ mK and $0.94\kappa_0 T$ at $T_0 = 45$ mK. So the change in the electron temperature of 12.5% corresponds to the 6% change in thermal conductance as shown in table S5. Since the inaccuracy in electron temperature is less than 4%, inaccuracy in extracted thermal conductance will be even much lesser than 6%. In device-3, the electron temperature T_0 was $\sim$ 27mK. Considering the maximum inaccuracy of 4% in electron temperature T_0, we have extracted the thermal conductance values of $\frac{4}{3}$ state at $T_0 = 27$ mK and 28mK. The values of thermal conductance were found $2.08\kappa_0 T$ at $T_0 = 27$ mK and $2.07\kappa_0 T$ at $T_0 = 28$ mK. So the change in electron temperature by $\sim 4\%$ does not change the extracted value of thermal conductance much. The extracted value of thermal conductance ($2.08\kappa_0 T$) is within $\sim 4\%$ inaccuracy of the theoretical value ($2\kappa_0 T$). The estimated shot noise due to the finite contact resistance in our device is at least one order of magnitude smaller compared to measured excess thermal noise as shown in table S3 and table S4. The heated up electrons must dwell in the floating reservoir for a time longer than the electron-electron energy relaxation time in order to achieve a quasi-equilibrium temperature T_M, which can be easily justified in our devices. Since the typical electron-electron interaction at low temperature is ~ 10 ns in gold like material(54), which is very much lower than typical dwell time (t_{dwell}) $\sim 20\ \mu s$ found in our devices. The t_{dwell} inside micron-size floating contact is evaluated from the equation $t_{dwell} = \frac{D_E \Omega h}{N}$ $(7, 55)$, with D_E the electronic density of states per unit volume per unit energy and Ω the volume of micron-size floating contact and N the number of channel leaving the floating contact. In our devices, for the typical volume of floating contact of $\approx 5\ \mu m^3$ and typical density of states for gold $D_E \simeq 1.14 \times 10^{47} J^{-1} m^{-3}$, we found $t_{dwell} \simeq \frac{40 \mu s}{N}$.

Table S5. Change in thermal conductance for different electron temperature T_0. The average value of electronic thermal conductance calculated from above table is the $(1.00 \pm 0.05)\kappa_0 T$ at $T_0 = 40$ mK and $(0.94 \pm 0.04)\kappa_0 T$ at $T_0 = 45$ mK. It is clear from above table that the change in the temperature of 12.5% corresponds to the 6% change in thermal conductance.

Device	Magnetic field B (T)	Configuration	Thermal Conductance g_Q (in unit of $\kappa_0 T$)	
			$T_0 = 40$ mK	$T_0 = 45$ mK
1	B = 9.8 T	ν = 1 and 2	0.96	0.90
		ν = 2 and 6	0.99	0.92
	B = 6.0 T	ν = 2 and 6	0.97	0.91
2	B = 6.0 T	ν = 2 and 6	1.08	1.01

Section S10. Discussion on heat Coulomb blockade

In device-3, the right value of the thermal conductance was obtained without varying the number of outgoing channels (ΔN) because of lack of electron-phonon coupling at lower temperatures below 60mK. However, it has been shown experimentally(39) that the heat Coulomb blockade can reduce the value of thermal conductance if the electron temperature of the floating contact is much lower than the crossover temperature (T_{CB}), where the $T_{CB} = \frac{\nu e^2}{\pi k_B C}$ is determined by the capacitance (C) of the floating contact. For device-3, graphite back gate is seperated from graphene by the bottom hBN of thickness $\sim$ 20 nm. Using the separation of $\sim$ 10 nm thick hBN (between the graphite back gate and floating contact determined from the reactive ion etching rate) and the area of floating contact of 8.2 μm^2, the geometrical capacitance of floating contact was found to be $\sim$ 29 fF. The crossover temperature T_{CB} for this value of capacitance was found to be $\sim$ 20 mK at $\nu = 1$, which is lower than the lowest electron temperature ($\sim$ 27mK) in our measurement. Thus, the contribution of the heat Coulomb blockade is expected to be neglisible for device 3. To estimate the contribution of heat Coulomb blockade, we have

used the following equation(39, 40)

$$J_Q^{CB}(N, T_M, T_0, E_C) = \frac{N^2 E_C^2}{\pi^2 h}\left[I\Big(\frac{NE_C}{\pi k_B T_0}\Big) - I\Big(\frac{NE_C}{\pi k_B T_M}\Big)\right] \tag{22}$$

where, $J_Q^{CB}(N, T_M, T_0, E_C)$ is the heat Coulomb blockade part of thermal current and $E_C = \frac{e^2}{2C}$ is the charging energy of floating contact and the function I is given by

$$I(x) = \frac{1}{2}\left[ln\Big(\frac{x}{2\pi}\Big) - \frac{\pi}{x} - \Psi\Big(\frac{x}{2\pi}\Big)\right] \tag{23}$$

where $\Psi(z)$ is digamma function. We have generated the dashed curve in Fig 3(b) of the manuscript using the Eqn. 22. It is clear from the theoretical curve that the effect of heat Coulomb blockade is negligible for device-3 in operated temperature regime. In device 1 and device 2, we have used the $\sim$ 300 nm of SiO_2 as dielectric. The area of floating contact in device-1 and device-2 were 5.7 μm^2 and 3.9 μm^2, respectively, which correspond to capacitance of 0.67 fF and 0.46 fF, respectively. For these values of capacitance the crossover temperatures T_{CB} were found to be $\sim$ 880 mK and $\sim$ 1.28 K for device 1 and device 2, respectively at $\nu = 1$. Since our operating temperature range is less than the calculated crossover temperature, one could expect the fully developed heat Coulomb blockade independent of the filling factor ν. However, there will be no impact on the extracted electronic thermal conductance values (by changing the number of channels - ΔN) shown in the Fig. 2(e) of the manuscript. Although it may affect the extracted electron-phonon contribution. To verify this, we have used $J_Q^{e-ph} = J_Q - J_Q^e$ with $J_Q^e = 0.5(N-1)\kappa_0(T_M^2 - T_0^2)$ and found temperature exponents closed to four for both the devices. These values are very similar to the values obtained in the section S8 (deviated by 5%). Thus, the effect of heat Coulomb blockade is not conclusive for the device 1 and device 2 in the present experiment and further investigations are required to study the heat Coulomb blockade in graphene.